nature nanotechnology

SUPPLEMENTARY INFORMATION

DOI: 10.1038/NNANO.2014.234

Nanotube mechanical resonators with quality factors of up to 5 million

J. Moser, A. Eichler, J. Güttinger, M. I. Dykman, and A. Bachtold

CONTENTS

I. CONDUCTANCE AS A FUNCTION OF GATE VOLTAGE

The conductance G as a function of gate voltage V_g^{DC} at 30 mK is shown in Supplementary Fig. S1. The regime for positive V_g^{DC} corresponds to Coulomb blockade (Supplementary Fig. S1b, middle and right-hand-side panels). Indeed, the length of the blockaded region, estimated to be ~ 1.5 μm from the separation between conductance oscillations, is close to the width of the trench (see next section). For negative V_g^{DC}, charge transport is in the so-called Fabry-Perot regime (Supplementary Fig. S1b, left-hand-side panel). The period in V_g^{DC} of the oscillations of G is a few times larger than the period of oscillations for positive V_g^{DC}, as usually observed for suspended nanotubes. In addition, the conductance is close to $2e^2/h$, indicating that the electronic transmission of each contact is high.

The measurement shown in Supplementary Fig. S1 is typical of ultra-clean nanotubes [1]. The regions of the nanotube near the metal electrodes remain p-doped, due to the work function of the electrodes, whereas the suspended part of the nanotube can be doped with electrons or holes using V_g^{DC}. For positive V_g^{DC}, $p-n$ junctions are formed near the metal electrodes, resulting in a Coulomb blockaded region along the suspended nanotube. For negative V_g^{DC}, the nanotube is p-doped along the whole tube and no tunnel barriers are formed. Near $V_g^{DC} = 0$, the conductance is zero because the Fermi energy lies inside the energy band gap along the entire suspended part of the nanotube.

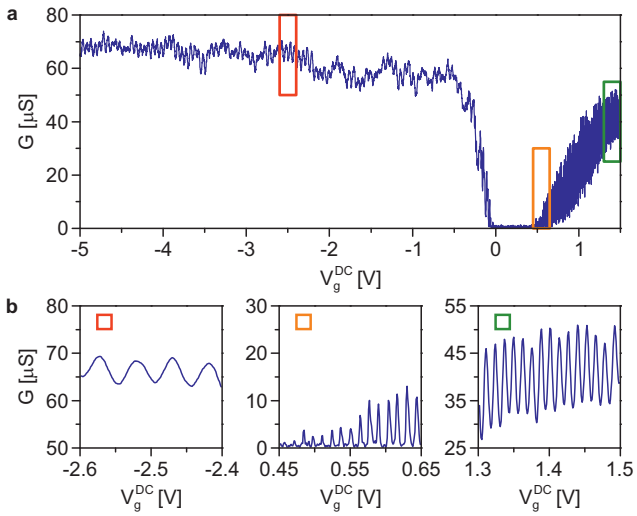

Figure S1. (a) Conductance G as a function of gate voltage V_g^{DC}. Regions within colored rectangles are blown up in (b).

II. ESTIMATING C_g'

We estimate the capacitance C_g between the nanotube and the gate from the separation $\Delta V_g^{DC} = 13 \pm 1$ mV between two conductance peaks in the Coulomb blockade regime (Supplementary Fig. S1b, central and right-hand-side panels): $C_g = e/\Delta V_g^{DC} = 1.2 \pm 0.1 \times 10^{-17}$ F. This value is close to the model capacitance between a cylinder of length L and radius r, and a plane a distance h away:

$$C_g = \frac{2\pi\epsilon_0 L}{\ln\left(\frac{2(h-z)}{r}\right)},$$

where ϵ_0 is the vacuum permittivity, h is the separation between the nanotube and the gate, and $z \ll h$ is a small displacement of the cylinder in the direction normal to the gate. The derivative dC_g/dz reads

$$C_g' = \left(\frac{dC_g}{dz}\right)_{z=0} = \frac{C_g}{h\ln(2h/r)} = (5.2 \pm 1.9) \times 10^{-12}\ \mathrm{F/m},$$

using $h = 350 \pm 50$ nm and $r = 1 \pm 0.5$ nm (the typical radius of nanotubes obtained with our chemical vapour deposition technique).

III. ESTIMATING THE EFFECTIVE MASS

We study the fundamental flexural mode of the nanotube resonator (see Fig. 1b of the main text). We use a simple model whereby the nanotube is straight and is perpendicular to the trench. The effective mass M of the mode is related to the mass of the nanotube M_{NT} as

$$M = M_{NT}\frac{1}{L}\int_0^L [\phi(x)]^2 dx,$$

where L is the length of the nanotube and $\phi(x)$ is the shape of the mode, which is normalized so that $\max[\phi(x)] = 1$. Given that mechanical tension is induced in the nanotube by the contacts and by the gate voltage, we assume that the modal shape is $\phi(x) = \sin(\pi x/L)$. The latter is the simplest approximation for the shape of a beam under tension. We emphasize that the expression for M takes into account the shape of the vibrational mode; all other quantities are measured with respect to the amplitude of this mode. To estimate M_{NT}, we also assume that the length of the nanotube is equal to the trench width ($L = 1.8 \pm 0.2$ μm)

and that $r = 1$ nm as in Section II. Therefore

$$M = \frac{1}{2}\left(2M_C \times \frac{2\pi r \times L}{A}\right) = (4.4 \pm 2.4) \times 10^{-21}\ \text{kg}\,,$$

where $M_C = 2 \times 10^{-26}$ kg is the mass of a carbon atom and $A = 5.2 \times 10^{-20}$ m^2 is the surface area of a hexagon in the honeycomb lattice of graphene.

IV. ORIENTATION OF THE MODE WITH RESPECT TO THE GATE ELECTRODE

The orientation of the vibrations of the eigenmode depends on the static curvature of the suspended nanotube, which builds in during the fabrication of the resonator. Since the static curvature cannot be controlled and cannot be accurately measured, the eigenmode can vibrate in any direction. For a real nanotube, the displacement along the nanotube can be quite complicated. However, we will use a simplified model where at least for the lowest mode the displacement is in one plane. We will characterize this plane by the angle θ it makes with the plane parallel to the surface of the gate electrode (Supplementary Fig. S2a).

We assume that current fluctuations δI at the drain electrode are proportional to motional fluctuations δz along the direction $\hat{z}$ normal to the gate electrode. Then, the current at the frequency close to the difference between the mode eigenfrequency and the frequency of the source-drain voltage is

$$\delta I = \beta \delta z = \frac{1}{2}\frac{dG}{dV_g} V_g^{DC} V_{sd}^{AC} \frac{C_g'}{C_g} \delta z\,, \tag{S1}$$

where dG/dV_g is the transcondutance, V_g^{DC} is the static gate voltage, and V_{sd}^{AC} is the amplitude of the oscillating source-drain voltage. We assume that the mode is polarized along $\hat{q}$, as shown in Supplementary Fig. S2a; hence, δz is the projection along $\hat{z}$ of the motional fluctuation δq along $\hat{q}$:

$$\delta z = \delta q \sin\theta\,, \tag{S2}$$

where θ is the angle between $\hat{y}$ and $\hat{q}$. To estimate θ, we subject the nanotube to a weak electrostatic force by applying a small oscillating voltage with amplitude δV_g^{AC} to the gate. The component of the force along $\hat{z}$ is $\delta F_z = C_g' V_g^{DC} \delta V_g^{AC}$. The center of mass of the nanotube experiences a force $\delta F_q = \delta F_z \sin\theta$, the projection of δF_z along $\hat{q}$. On resonance,

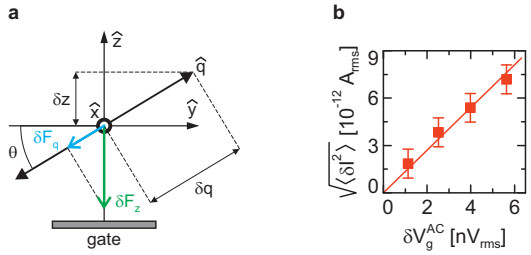

Figure S2. (a) Orientation of the displacement for a simple model of a straight nanotube parallel to the gate electrode. $\hat{x}$ and $\hat{y}$ are parallel to the gate, and $\hat{z}$ is normal to the gate. The displacement (that is, the mode polarization) is along $\hat{q}$. The force δF_z along $\hat{z}$ acts on the motion of the nanotube through the force δF_q, its projection onto $\hat{q}$. The projection of displacement δq onto $\hat{z}$ is δz. (b) Standard deviation of current $\sqrt{\langle \delta I^2 \rangle}$ induced by a small oscillating gate voltage of amplitude δV_g^{AC} applied on resonance. δV_g^{AC} produces the force δF_z in (a).

the displacement δq induced by δF_q reads

$$\delta q = \frac{Q}{M\omega_0^2}\delta F_q \,, \tag{S3}$$

where Q is the quality factor of the resonance, M the effective mass, and $\frac{\omega_0}{2\pi}$ the resonant frequency. In turn, the displacement δq induces current oscillations of variance $\langle \delta I^2 \rangle$ at the drain:

$$\sqrt{\langle \delta I^2 \rangle} = \beta \sin^2\theta \frac{Q}{M\omega_0^2} C_g' V_g^{DC} \delta V_g^{AC} = p \delta V_g^{AC} \,. \tag{S4}$$

Supplementary Fig. S2b shows $\sqrt{\langle \delta I^2 \rangle}$ as a function of δV_g^{AC}, measured with the technique described in the main text and in Ref. [2]. The dependence of $\sqrt{\langle \delta I^2 \rangle}$ on δV_g^{AC} is linear and extrapolates to zero in the limit of zero δV_g^{AC}, as expected from Eq (S4). We obtain $\theta = 60° \pm 25°$ from the slope in Supplementary Fig. S2b, using $|V_g^{DC}| = 2.2$ V, $V_{sd}^{AC} = 3.17 \times 10^{-4}$ V, $C_g = (1.2 \pm 0.1) \times 10^{-17}$ F, $C_g' = (5.2 \pm 1.9) \times 10^{-12}$ F/m, $M = (4.4 \pm 2.4) \times 10^{-21}$ kg, $\omega_0/(2\pi) = 44.1 \times 10^6$ Hz, $Q = 5 \times 10^5$, $dG/dV_g = 6.4 \times 10^{-4}$ S/V, and $p = (1.3 \pm 0.2) \times 10^{-3}$ A/V.

The estimation of θ comes with a large uncertainty that mostly originates from the uncertainties in the estimations of C_g' and M. These uncertainties, however, have little impact on the estimation of the modal temperature T, which we present is Section V. Indeed, we show that T is proportional to $M/(C_g' \sin\theta)^2$, a quantity that we can estimate rather precisely from the measurement shown in Supplementary Fig. 2b. For this, we rewrite

Eq. (S4) as:

$$\frac{M}{(C_g' \sin\theta)^2} = \frac{1}{p}\left(\frac{1}{2}\frac{dG}{dV_g}(V_g^{DC})^2 V_{sd}^{AC}\frac{1}{C_g}\frac{Q}{\omega_0^2}\right). \tag{S5}$$

Using the values given above, we calculate the right-hand-side of Eq. (S5) and obtain

$$\frac{M}{(C_g' \sin\theta)^2} = 205 \pm 40 \text{ kg}\cdot\text{m}^2/\text{F}^2 .$$

We use this value to estimate T is Section V.

V. MODE TEMPERATURE

Using Eqs. (S1) and (S2), the equipartition theorem yields

$$k_B T = M\omega_0^2\langle\delta q^2\rangle = M\omega_0^2\frac{1}{(\beta\sin\theta)^2}\frac{1}{2\pi}\int_{-\infty}^{\infty} S_I(\omega)d\omega , \tag{S6}$$

where $\langle\delta q^2\rangle$ is the variance of displacement along $\hat{q}$, and $S_I(\omega)$ is the *two-sided* power spectral density of current fluctuations δI. To make contact with the experiment, we also express $k_B T$ in terms of $S_I(2\pi f)$, where $f = \frac{\omega}{2\pi}$ is the natural frequency:

$$k_B T = M\omega_0^2\frac{1}{(\beta\sin\theta)^2}\int_0^{\infty} 2S_I(2\pi f)df , \tag{S7}$$

where we used

$$\frac{1}{2\pi}\int_{-\infty}^{\infty} S_I(\omega)d\omega = \int_{-\infty}^{\infty} S_I(2\pi f)df = 2\int_0^{\infty} S_I(2\pi f)df .$$

In Eq. (S7), $S_I(2\pi f)$ is defined as

$$S_I(2\pi f) = \lim_{\tau\to\infty}\int_{-\tau/2}^{\tau/2}\langle\delta I(t)\delta I(0)\rangle\exp[-i(2\pi f + \omega_{sd} - \omega_0)t]dt , \tag{S8}$$

where τ is the measurement time, ω_{sd} is the off-resonance angular frequency of the source-drain voltage, and ω_0 is the resonant angular frequency. Experimentally, we measure the *single-sided* power spectral density $S_I^{\text{exp}}(2\pi f) = 2S_I(2\pi f)$.

We estimate the mode temperature T from the power spectra in Figs. 2e,f of the main text. We obtain $T \simeq 44 \pm 10$ mK, using the following parameters: $|V_g^{DC}| = 3.037$ V, $dG/dV_g = 8.5\times10^{-4}$ S/V, $V_{sd}^{AC} = 4\times10^{-4}$ V, $C_g = (1.2\pm0.1)\times10^{-17}$ F, $\omega_0/(2\pi) = 55.6\times10^6$ Hz, and $\int_0^{\infty} S_I^{\text{exp}}(2\pi f)df = 4.5\times10^{-23}$ A^2. We also use $M/(C_g'\sin\theta)^2 = 205\pm40$ kg$\cdot$m^2/F^2 obtained in Section IV.

We were not able to carry out a temperature dependence of $\langle\delta z^2\rangle$. Connecting thermometry lines to the cryostat would generate electrical noise in our measurement, masking the mechanical resonance in the spectra.

VI. DEPENDENCES OF THE RESONANT FREQUENCY AND THE Q-FACTOR ON DC GATE VOLTAGE

Supplementary Fig. S3a shows the resonant frequency as a function of V_g^{DC} obtained by measuring the mixing current I_{mix} with the FM technique [3] as a function of V_g^{DC} and drive frequency f. The intensity of I_{mix} varies with V_g^{DC} because it is proportional to the transconductance. The resonant frequency f_0 is linear in V_g^{DC}. Supplementary Fig. S3c shows the inverse of the Q-factor as V_g^{DC} is stepped from the bottom of an oscillation in $I^{DC}(V_g^{DC})$ to the top of this oscillation. No variation of $1/Q$ is seen.

The dependences of f_0 and $1/Q$ on V_g^{DC} are different from what is observed in nanotube resonators operated in the Coulomb blockade regime. There, the resonator experiences a reduction of f_0 near the top of an oscillation in I^{DC} as a function of V_g^{DC}. In addition, $1/Q$ is higher near the top of the oscillation in I^{DC} because electron tunneling events are accompanied by enhanced dissipation. The absence of such behaviors demonstrates that the effect of the coupling between vibrations and Coulomb blockade is weak in our experiment.

VII. EFFECT OF ELECTROSTATIC WHITE NOISE ON THE SPECTRUM OF THE RESONATOR.

Figure 3f of the main text displays $1/Q$ in the presence of gate voltage noise of various intensities. The gate voltage noise is applied using the Johnson-Nyquist noise of a 50 Ohm resistor at room temperature amplified by different gains (by varying the number of amplifiers). We measure the power spectral density of the amplified Johnson-Nyquist noise with a signal analyzer in a separate experiment. We verify that this amplified noise is white (the power spectral density is constant) between 1 MHz and 200 MHz, a frequency range that encompasses the resonant frequency of our resonator (40-60 MHz). Noise at frequencies below 1 MHz is cut off by a high pass filter at the sample stage. The power spectral densities we measure are consistent with the gain (20 dB) and the noise figure (1 dB) of each amplifier used in combination with the total attenuation along our radio frequency lines.

The applied Johnson-Nyquist noise creates a random electrostatic force between the nanotube and the gate (top axis of Fig. 3f). To the lowest order in the nanotube displacement,

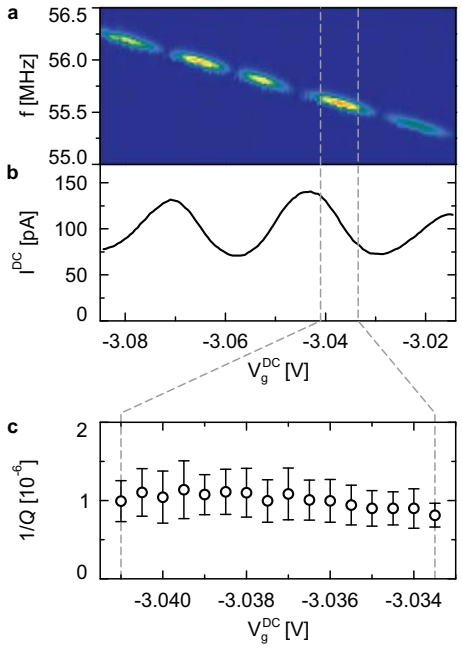

Figure S3. (a) Electro-mechanical mixing current measured with the FM technique, as a function of V_g^{DC} and drive frequency f. Scale bar from blue, 1 pA, to orange, 140 pA. (b) Source-drain DC current I^{DC} as a function of V_g^{DC}, showing Fabry-Perrot oscillations. (c) $1/Q$ as a function of time averaged V_g^{DC}. Measurement time is 6.3 s. The error bars correspond to the distribution of Q-factors for 20 power spectra.

this force is additive, which means that it is independent of the displacement. The nanotube resonator responds primarily to the frequency components of this force, which lie within the band centered at the resonant frequency, with the typical bandwidth given by the mechanical linewidth. The power spectrum of the random force is flat in this region, and therefore the corresponding noise is white. Its intensity S_{ef} is related to the power spectral density of the Johnson-Nyquist noise S_{JN} as $S_{ef} = (C_g' V_g^{DC} \sin\theta)^2 S_{JN}$ (see Section IV). We use $C_g' = 5.2 \times 10^{-12}$ F/m, $V_g^{DC} = 2.2$ V, and $\theta = 60°$.

The effect of the additive Johnson-Nyquist noise is fully analogous to the effect of the thermal noise that comes along with the resonator dissipation. It leads to the increase of the intensity of the peak in the resonator power spectrum and to spectral broadening of this peak via nonlinear damping and via the dependence of the oscillator frequency on the vibration amplitude.

The low-frequency components of the Johnson-Nyquist noise could directly lead to fluc-

tuations of the resonator frequency, which would be similar to the low-frequency fluctuations induced by the voltage noise of the DC voltage source. They would come from the dependence of the resonator frequency on the gate voltage. Such noise is multiplicative, since the corresponding force is proportional to the resonator displacement, and this is why it acts as a frequency shift. The resonator responds to such noise if its frequencies are low, within the typical bandwidth given by the mechanical linewidth. Higher-frequency components are averaged out. For the Johnson-Nyquist noise that we are using the effect of this noise is very weak, because the initial noise from the 50 Ohm resistor is only weakly amplified below 100 kHz, and is further attenuated by a high-pass filter below 10 kHz. We estimate that the corresponding gate voltage fluctuations induce a lineshape broadening of only a fraction of a Hertz, much smaller than the linewidths we measure in Fig. 3f.

VIII. VOLTAGE FLUCTUATIONS OF THE DC VOLTAGE SOURCES

The voltage fluctuations of both the Keithley source and of the lead battery are measured in a separate experiment. The DC source is connected to the DC gate voltage input port outside of the cryostat. A finite DC voltage close to the gate voltages used in the main text is applied. The voltage fluctuations at 300 K are measured at the sample stage after opening the cryostat. These fluctuations are recorded with a voltmeter as a function of time (Supplementary Fig. S4). The measured voltage fluctuations are larger than the intrinsic readout fluctuations of the voltmeter. These measurements are used to estimate the Allan deviation in Figs. 3c,d (blue traces) of the main text.

IX. ADDITIONAL SAMPLE

We investigated a second nanotube resonator device operated in the Fabry-Perot regime at a refrigerator temperature of 30 mK. An example of a high Q resonance for this device is shown in Supplementary Fig. S5. The parameters used for this measurement are: $V_g^{DC} = -3.643$ V, $V_{sd}^{AC} = 4 \times 10^{-4}$ V, and a measurement time of 4.8 s. The measurements were carried out with the Keithley source.

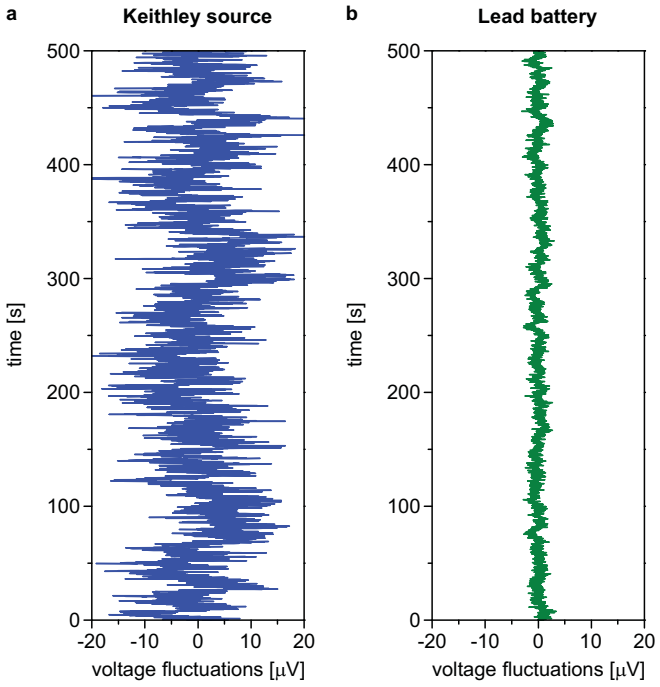

Figure S4. Gate voltage fluctuations measured at the sample stage. (a) Keithley source. (b) Lead battery.

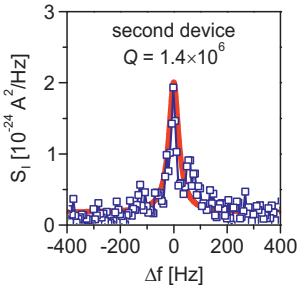

Figure S5. High Q resonance obtained with an additional device. The resonant frequency is $f_0 \simeq 62 \times 10^6$ Hz.

X. POWER SPECTRUM FOR A FINITE MEASUREMENT TIME

Below, power spectral densities are all *two-sided*. The power spectrum of displacement fluctuations for a finite measurement time τ reads

$$S_q(\omega) = \frac{1}{\tau}\int_0^\tau dt \int_0^\tau dt_1\, q(t)q(t_1)e^{i\omega(t-t_1)} = \frac{2}{\tau}\mathrm{Re}\int_0^\tau dt \int_0^t dt_1\, q(t)q(t_1)e^{i\omega(t-t_1)}\,. \qquad \text{(S9)}$$

We make the change from fast oscillating variables $q(t)$, $\dot{q}(t)$ to slow complex oscillator amplitude $u(t)$

$$\begin{aligned} q(t) &= u(t)e^{i\omega_0 t} + \text{c.c.}\,, \\ \dot{q}(t) &= i\omega_0 \left(ue^{i\omega_0 t} - u^* e^{-i\omega_0 t}\right)\,. \end{aligned} \tag{S10}$$

Plugging Eqs. (S10) into the equation of motion $\ddot{q} + 2\Gamma\dot{q} + [\omega_0^2 + 2\omega_0\xi(t)]q = f_T(t)/M$, and solving for u in the rotating wave approximation, we obtain

$$u(t) = \int_{-\infty}^{t} dt' \, \exp\left[-\Gamma(t-t') + i\int_{t'}^{t} \xi(t'')dt''\right] f_u(t')\,. \tag{S11}$$

In the above expression, ξ is the frequency noise, $f_u = 1/(2iM\omega_0)f_T(t)\exp(-i\omega_0 t)$ is the thermal noise with correlator $\langle f_u(t) f_{u^*}(t')\rangle = \frac{\Gamma k_B T}{M\omega_0^2}\delta(t-t')$, and M is the modal mass. Using Eqs. (S10) and (S11) along with Eq. (S9), we obtain

$$\begin{aligned} S_q(\omega) &= \frac{2}{\tau}\text{Re}\int_0^\tau dt \int_0^t dt_1 \, u^*(t)u(t_1)\exp\left[i(\omega-\omega_0)(t-t_1)\right] \\ &= \frac{2}{\tau}\text{Re}\int_0^\tau dt \int_0^t dt_1 \int_{-\infty}^{t} dt' \int_{-\infty}^{t_1} dt_1' \Bigg\{ \exp\left[i(\omega-\omega_0)(t-t_1) - \Gamma(t-t') - \Gamma(t_1-t_1')\right] \\ &\quad \times \exp\left[-i\int_{t'}^{t}\xi(t'')dt'' + i\int_{t_1'}^{t_1}\xi(t_1'')dt_1''\right] \times \frac{\Gamma k_B T}{M\omega_0^2}\delta(t'-t_1')\Bigg\} \\ &= \frac{\Gamma k_B T}{M\omega_0^2}\frac{2}{\tau}\text{Re}\int_0^\tau dt \int_0^t dt_1 \int_{-\infty}^{t_1} dt' \Bigg\{ \exp\left[i(\omega-\omega_0)(t-t_1) - \Gamma(t+t_1-2t')\right] \\ &\quad \times \exp\left[-i\int_{t_1}^{t}\xi(t'')dt''\right]\Bigg\} \\ &= \frac{k_B T}{M\omega_0^2}\frac{1}{\tau}\text{Re}\int_0^\tau dt \int_0^t dt_1 \, \exp\left[i(\omega-\omega_0)(t-t_1) - \Gamma(t-t_1) - i\int_{t_1}^{t}\xi(t'')dt''\right]\,. \end{aligned} \tag{S12}$$

In Eq. (S12), we average over thermal noise since its correlation time is short on the scale $\Gamma^{-1} \ll \tau$. We can now separate $\xi(t)$ into two parts, one slow and the other fast on the scale of the ring-down time Γ^{-1}: $\xi(t) = \xi_{slow}(t) + \xi_{fast}(t)$. We assume that ξ_{fast} is δ-correlated, which allows to simplify the power spectrum in Eq. (S12) as

$$\begin{aligned} S_q(\omega) &= \frac{k_B T}{M\omega_0^2}\frac{1}{\tau}\text{Re}\int_0^\tau dt \int_0^t dt_1 \, \exp\left\{\left[i(\omega-\tilde{\omega}_0) - \tilde{\Gamma}\right](t-t_1) - i\xi_{slow}(t)(t-t_1)\right\} \\ &= \frac{k_B T}{M\omega_0^2}\frac{1}{\tau}\int_0^\tau dt \, \frac{\tilde{\Gamma}}{\tilde{\Gamma}^2 + [\omega - \tilde{\omega}_0 - \xi_{slow}(t)]^2}\,, \qquad |\omega-\omega_0| \ll \omega_0\,, \end{aligned} \tag{S13}$$

where $\tilde{\Gamma}$ is the "instantaneous" half-width of the spectrum and $\tilde{\omega}_0$ is the resonant angular frequency, both renormalized by fast frequency noise. The relation between Γ and $\tilde{\Gamma}$ can be found in Supplementary Ref. [4]. Equation (S13) is Eq. (2) in Methods. The resonant peak corresponding to $S_q(\omega)$ only exists for $\exp\left(-\tilde{\Gamma}\tau\right) \ll 1$; the fact that resonance lineshapes remain close to Lorentzian indicates that our measurement times exceed $1/\tilde{\Gamma}$.

We emphasize that $\xi_{fast}(t)$ is δ-correlated on the "slow" time scale $\sim \Gamma^{-1}$, not on the fast scale $\sim \omega_0^{-1}$. It is seen from Eq. (S12) that the components of $\xi(t)$ with frequencies much higher than Γ are averaged out and therefore can be disregarded, as we indicated earlier. The case where the frequency noise has significant intensity near $2\omega_0$, so that it parametrically excites the resonator, requires a separate analysis, but we have no indications and no physical reasons to expect that strong frequency noise with frequencies $\approx 2\omega_0$ is present in our case.

The separation of the frequency noise into parts that are slow and fast on the time scale $1/\Gamma$ leaves out a comparatively narrow part of the noise spectrum. This part is averaged out when, as in our case, the duration of a measurement $\tau \gg 1/\Gamma$. It is reasonable to expect that the contribution of this narrow range of the frequency noise spectrum is small. Additional information about the spectrum of the frequency noise can be obtained by studying the power spectrum of the resonator in the presence of periodic modulation [4].

The integral width of the spectrum can be obtained from Eq. (S13). The integral width is expressed as the ratio $\mathcal{I} = \mathcal{A}/S_q^{\max}(\omega)$, where $\mathcal{A} = \int_0^\infty S_q(\omega)d\omega$ is the spectrum area and $S_q^{\max}(\omega)$ is the resonance height in the spectrum. The area $\mathcal{A} = \pi k_B T/(M\omega_0^2)$ is independent of frequency noise or decay rate. For a Lorentzian spectrum ($\xi_{slow} = 0$) we have

$$\mathcal{I}^{-1} = \frac{1}{\pi\tilde{\Gamma}} = Q\frac{2}{\pi\tilde{\omega}_0}\,,$$

where Q is the quality factor.

Next, we calculate $\mathcal{I}^{-1}$, a good number to characterize Q for asymmetric and noisy resonances. For slow frequency noise of weak intensity, the expression for the reciprocal width takes on a "finite-time variance" form:

$$\mathcal{I}^{-1} \simeq \frac{1}{\pi\tilde{\Gamma}}\left(1 - \frac{1}{\tilde{\Gamma}^2}\left[\frac{1}{\tau}\int_0^\tau dt\,\xi_{slow}^2(t) - \left(\frac{1}{\tau}\int_0^\tau dt\,\xi_{slow}(t)\right)^2\right]\right)\,, \tag{S14}$$

where $\frac{1}{\tau}\int_0^\tau dt\,\xi_{slow}(t)$ is the measured shift of the resonant frequency resulting from slow frequency noise. The term in square brackets in Eq. (S14) is always positive, resulting in the two following effects:

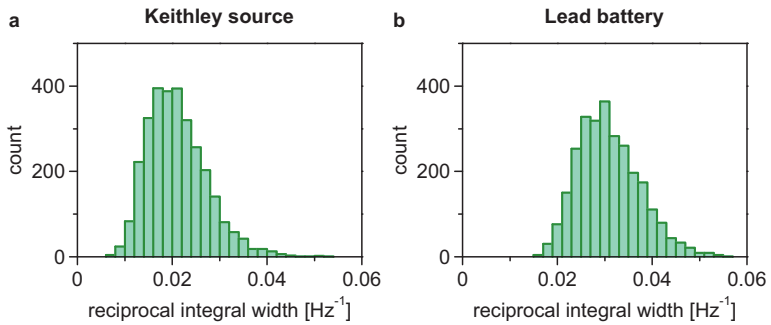

Figure S6. Histograms of the reciprocal integral width $\mathcal{I}^{-1}$, using the Keithley source (a) and the lead battery (b) to bias the gate electrode.

1. For a fixed measurement time τ, multiple measurements of the integral width give an asymmetric distribution of $\mathcal{I}^{-1}$;

2. As τ increases, the peak value of the distribution of $\mathcal{I}^{-1}$ decreases, whereas the mean $\mathcal{I}$ increases. Once τ exceeds the noise correlation time, $\mathcal{I}$ levels off to the value $\pi\tilde{\Gamma}\left(1+\frac{1}{\tilde{\Gamma}^2}\langle\xi^2_{slow}(t)\rangle\right)$.

Supplementary Fig. S6 shows histograms of $\mathcal{I}^{-1}$ built from the spectra used to construct the histograms in Figs. 2c,d of the main text. If, as we assume, the modulation of the conductance is linear in the resonator displacement, the current-to-displacement scaling coefficient drops out from $\mathcal{I}$. Therefore, the value of $\mathcal{I}$ can be found directly from the data on the current power spectra. Histograms of $\mathcal{I}^{-1}$ are asymmetric, in agreement with effect (1) predicted above. In addition, Fig. 3a of the main text shows that the peak value of the linewidth distribution tends to level off for long measurement times, in agreement with effect (2). (From that figure, we infer that the spectrum of the frequency noise has a cutoff around 1/20 Hz.) Slow fluctuations of the decay rate and/or the intensity of the thermal noise would not lead to the observed increase of the the peak value of the linewidth distribution with measurement time, but rather would cause $\mathcal{I}$ to decrease.

---

[1] Benyamini, A., Hamo, A., Viola Kusminskiy, S., von Oppen, F. & Ilani, S. Real-space tailoring of the electronphonon coupling in ultraclean nanotube mechanical resonators. *Nature Physics* **10**, 151-156 (2014).

[2] Moser, J., Güttinger, J., Eichler, A., Esplandiu, M. J., Liu, D. E., Dykman, M. I. & Bachtold, A. Ultrasensitive force detection with a nanotube mechanical resonator. *Nature Nanotech.* **8**, 493-496 (2013).

[3] Eichler, A., Moser, J., Chaste, J., Zdrojek, M., Wilson-Rae, I. & Bachtold, A. Nonlinear damping in mechanical resonators made from carbon nanotubes and graphene. *Nature Nanotech.* **6**, 339-342 (2011).

[4] Zhang, Y., Moser, J., Güttinger, J., Bachtold, A. & Dykman, M. I. Interplay of driving and frequency noise in the spectra of vibrational systems. *arXiv*:1406.1406

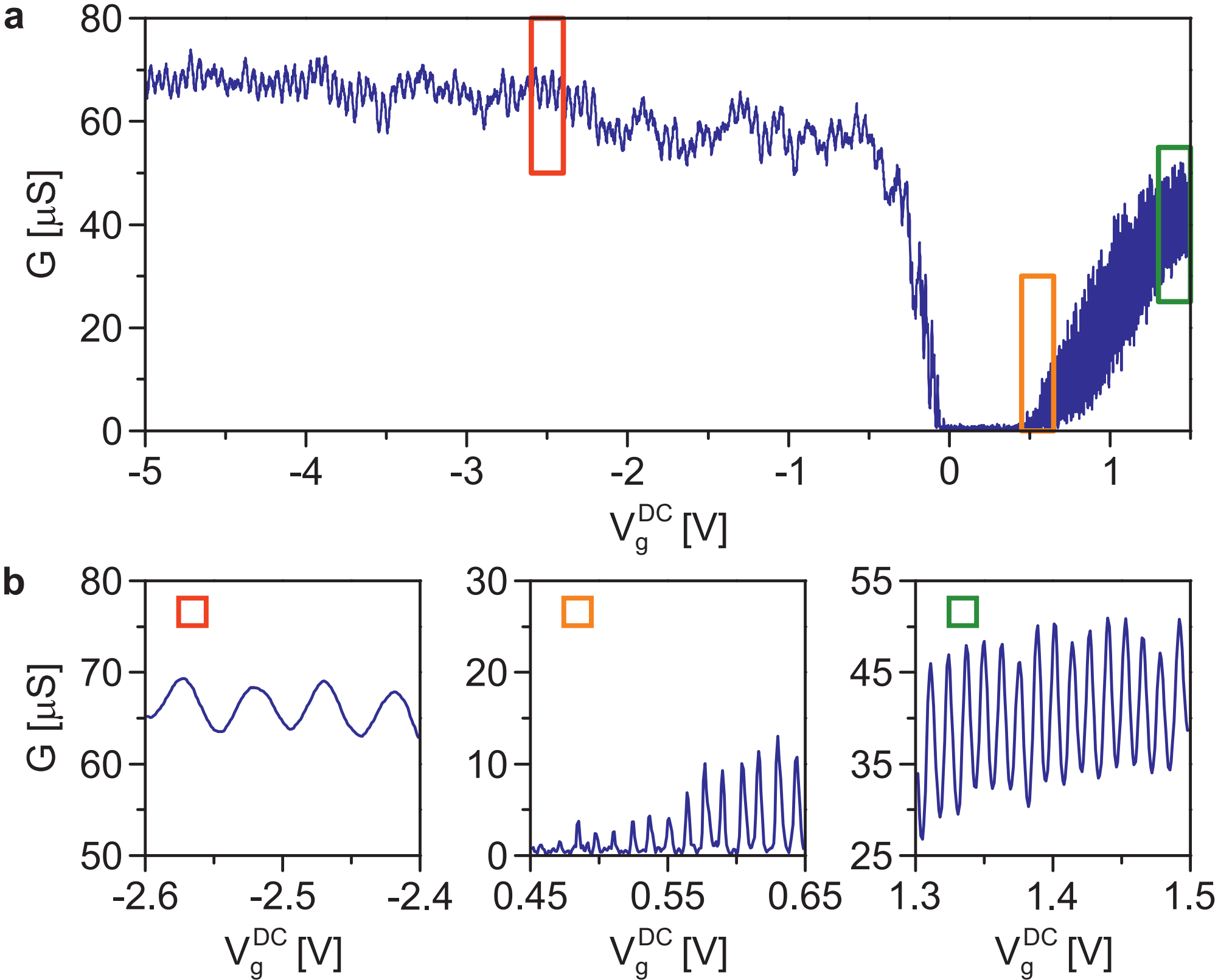
a
80
60
40
20
0
G [μS]
-5
-4
-3
-2
-1
0
1
V_g^{DC} [V]
b
80
70
60
50
G [μS]
-2.6
-2.5
-2.4
V_g^{DC} [V]
30
20
10
0
0.45
0.55
0.65
V_g^{DC} [V]
55
45
35
25
1.3
1.4
1.5
V_g^{DC} [V]

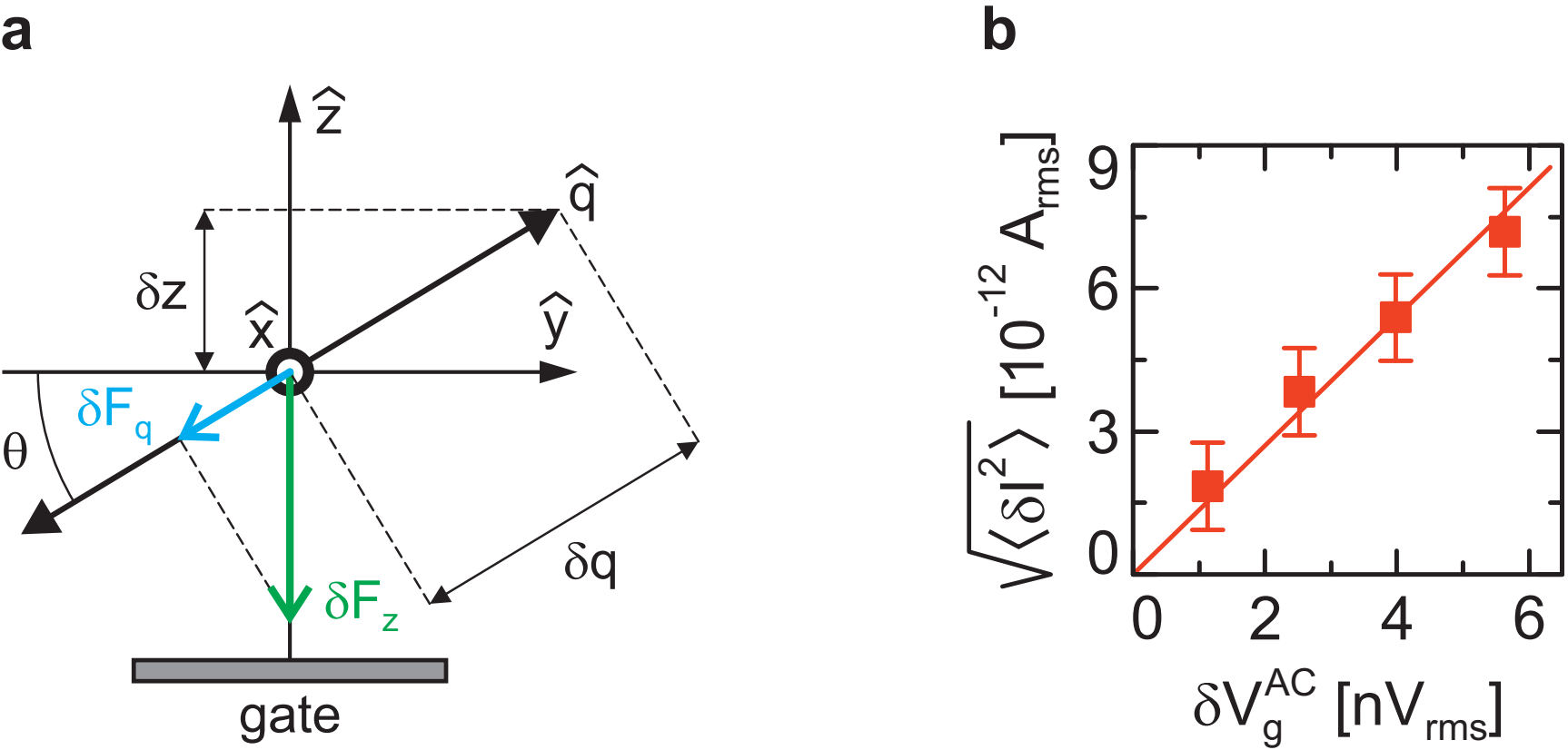
a
$\hat{z}$
$\hat{q}$
$\hat{x}$
$\hat{y}$
δz
θ
δF_q
δF_z
δq
gate
b
$\sqrt{\langle \delta I^2 \rangle}$ [10^{-12} A_{rms}]
0
3
6
9
0
2
4
6
δV_g^{AC} [nV_{rms}]

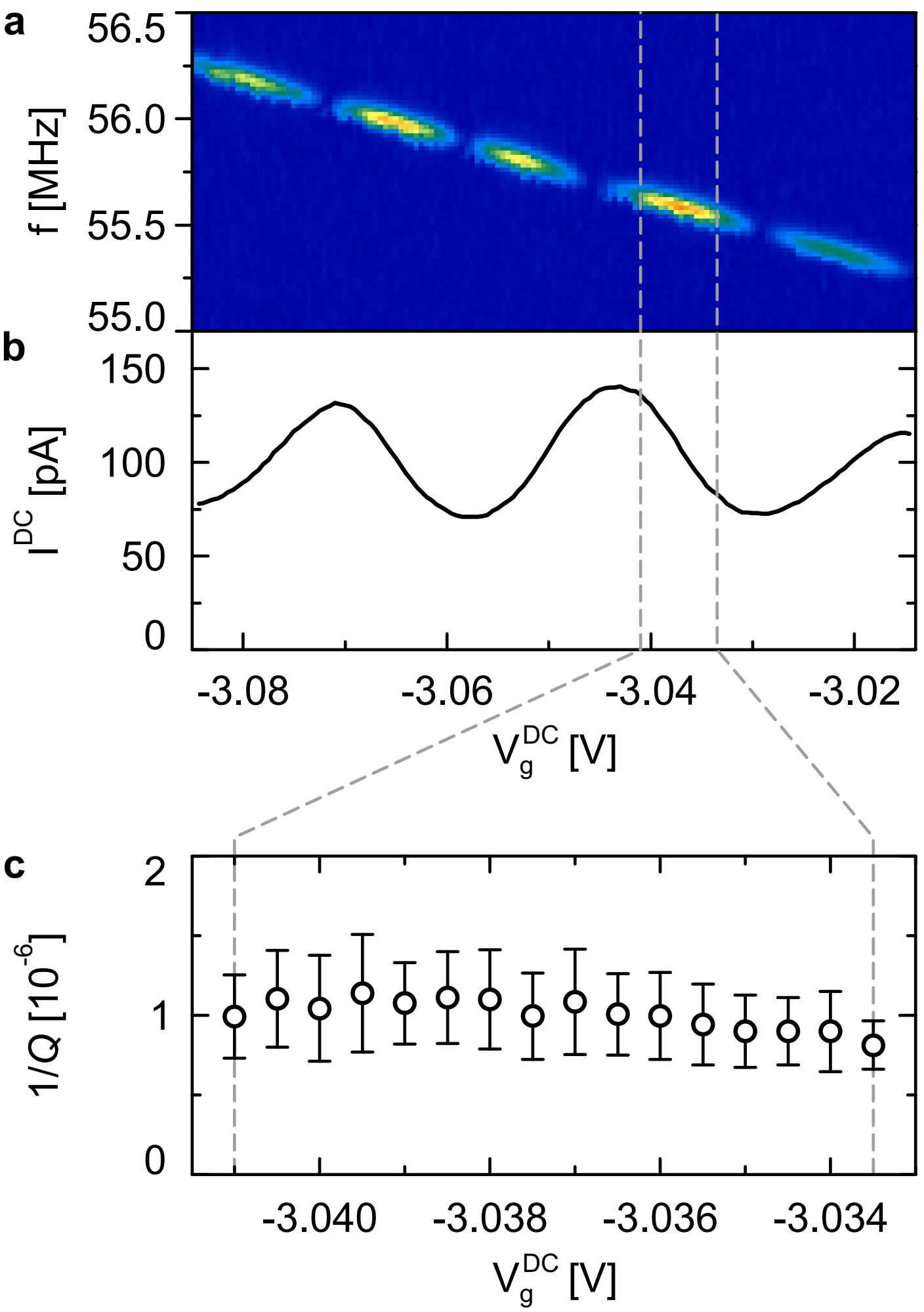
a
56.5
56.0
55.5
55.0
f [MHz]
b
150
100
50
0
I^{DC} [pA]
-3.08
-3.06
-3.04
-3.02
V_g^{DC} [V]
c
2
1
0
1/Q [10^{-6}]
-3.040
-3.038
-3.036
-3.034
V_g^{DC} [V]

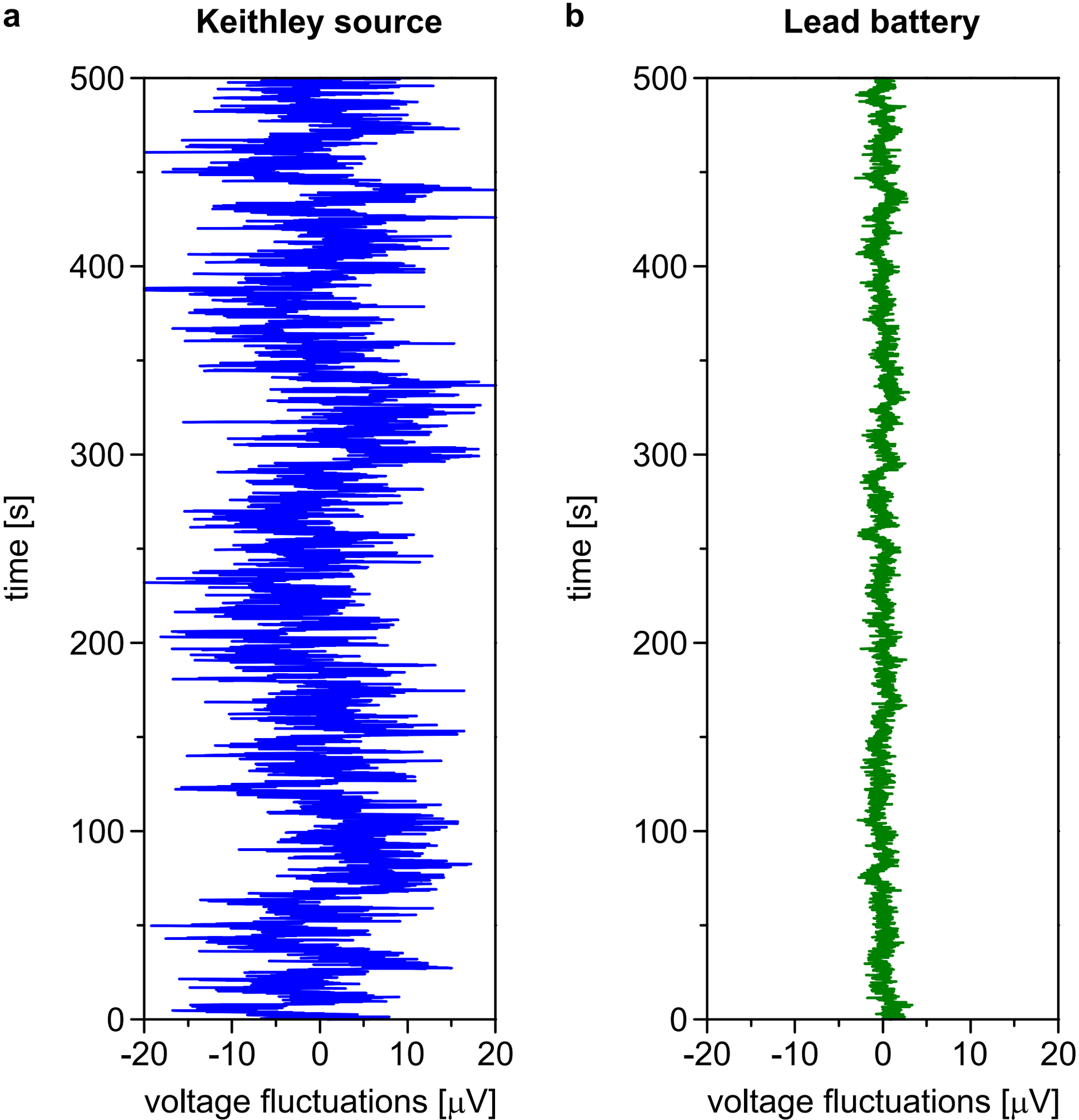
a
Keithley source
b
Lead battery
time [s]
time [s]
0
100
200
300
400
500
-20
-10
0
10
20
voltage fluctuations [μV]
voltage fluctuations [μV]

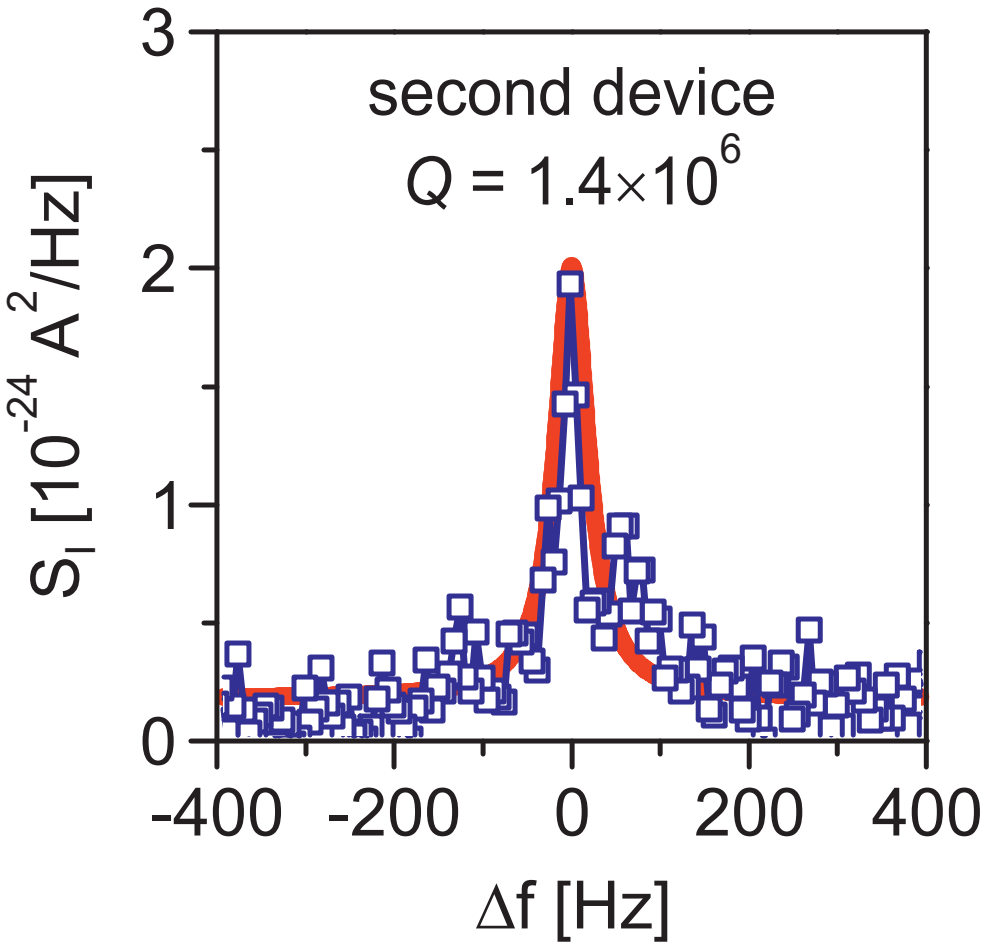
second device
Q = 1.4×10^6
S_I [10^-24 A^2/Hz]
Δf [Hz]
0
1
2
3
-400
-200
0
200
400

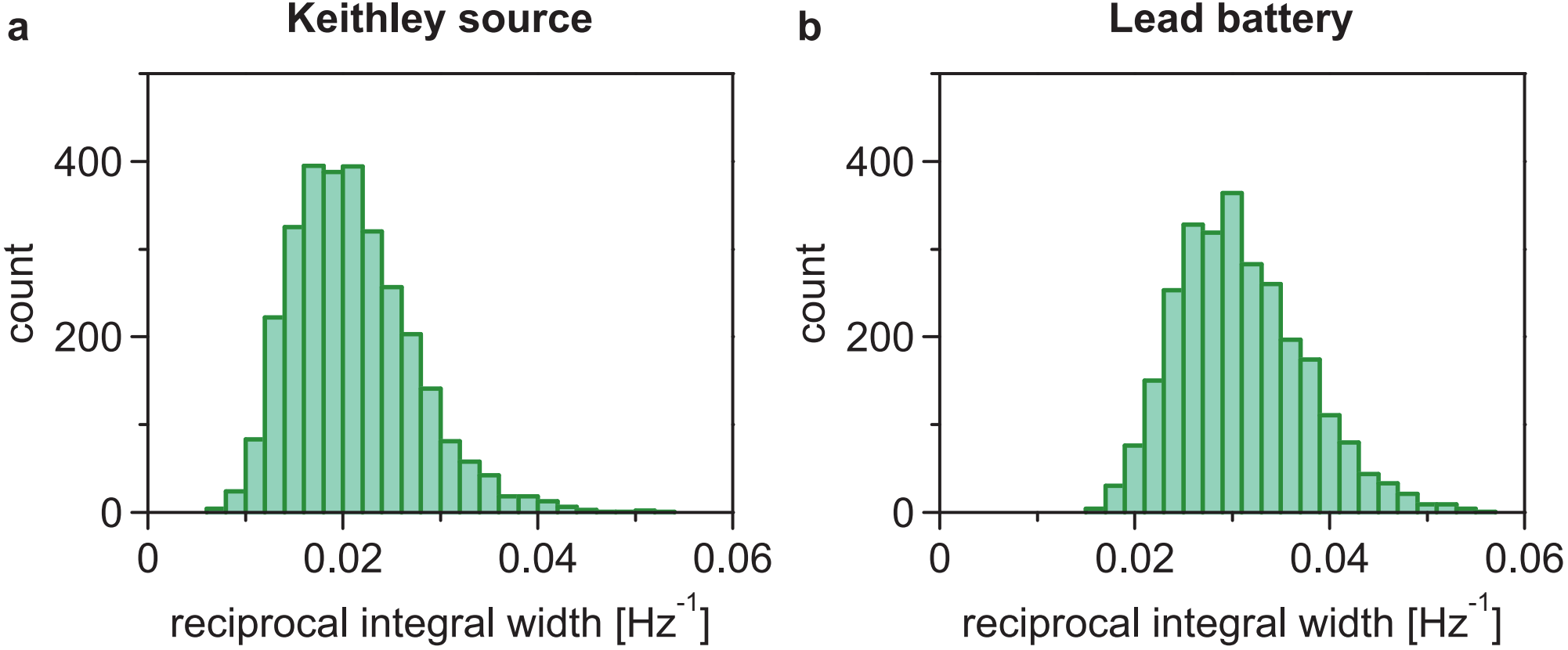
a
Keithley source
count
400
200
0
0
0.02
0.04
0.06
reciprocal integral width [Hz^{-1}]
b
Lead battery
count
400
200
0
0
0.02
0.04
0.06
reciprocal integral width [Hz^{-1}]